AD-A086 426 OHIO STATE UNIV COLUMBUS ELECTROSCIENCE LAB F/G 20/14
PATTERN ANALYSIS OF A HORN ANTENNA IN THE PRESENCE OF OBSTACLES--ETC(U)
FEB 80 W D BURNSIDE, C S KIM N62269-78-C-0370
UNCLASSIFIED ESL-711588-1 NADC-80095-30 NL

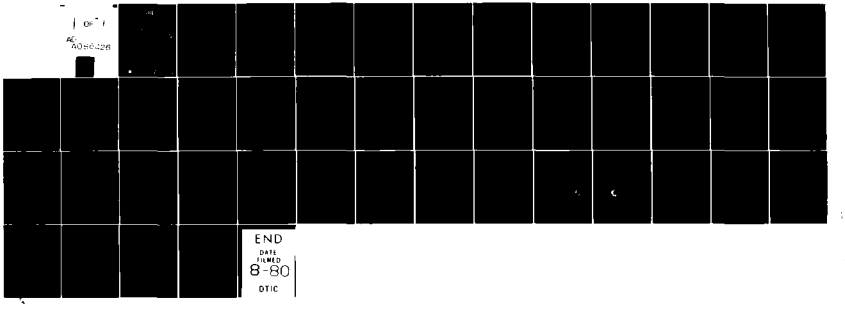

END
DATE FILMED
8-80
DTIC

NADC-80095-30

LEVEL II

F 12

OSU

The Ohio State University

PATTERN ANALYSIS OF A HORN ANTENNA IN THE PRESENCE OF OBSTACLES

W. D. Burnside and C. S. Kim

The Ohio State University

ElectroScience Laboratory

Department of Electrical Engineering
Columbus, Ohio 43212

Technical Report 711588-1

Contract N62269-78-C-0379

February 1980

NOTICES

When Government drawings, specifications, or other data are used for any purpose other than in connection with a definitely related Government procurement operation, the United States Government thereby incurs no responsibility nor any obligation whatsoever, and the fact that the Government may have formulated, furnished, or in any way supplied the said drawings, specifications, or other data, is not to be regarded by implication or otherwise as in any manner licensing the holder or any other person or corporation, or conveying any rights or permission to manufacture, use, or sell any patented invention that may in any way be related thereto.

SECURITY CLASSIFICATION OF THIS PAGE *(When Data Entered)*

REPORT DOCUMENTATION PAGE

READ INSTRUCTIONS BEFORE COMPLETING FORM

1. REPORT NUMBER: NADC-80095-30	2. GOVT ACCESSION NO.
3. RECIPIENT'S CATALOG NUMBER	
4. TITLE *(and Subtitle)*: PATTERN ANALYSIS OF A HORN ANTENNA IN THE PRESENCE OF OBSTACLES.	5. TYPE OF REPORT & PERIOD COVERED: Technical Report.
6. PERFORMING ORG. REPORT NUMBER: ESL-711588-1	
7. AUTHOR(s): W. D. Burnside, C. S. Kim	8. CONTRACT OR GRANT NUMBER(s): N62269-78-C-0379
9. PERFORMING ORGANIZATION NAME AND ADDRESS: The Ohio State University ElectroScience Laboratory, Department of Electrical Engineering, Columbus, Ohio 43212	10. PROGRAM ELEMENT, PROJECT, TASK AREA & WORK UNIT NUMBERS: 63206N, W0638TW, W06380000, RA705
11. CONTROLLING OFFICE NAME AND ADDRESS: Naval Air Development Center, Warminster, Pennsylvania 18974	12. REPORT DATE: February 1980
	13. NUMBER OF PAGES: 44
14. MONITORING AGENCY NAME & ADDRESS *(if different from Controlling Office)*	15. SECURITY CLASS. *(of this report)*: Unclassified
	15a. DECLASSIFICATION/DOWNGRADING SCHEDULE

16. DISTRIBUTION STATEMENT *(of this Report)*

Approved for public release; distribution unlimited.

16 W0638000, W0638TW

17. DISTRIBUTION STATEMENT *(of the abstract entered in Block 20, if different from Report)*

18. SUPPLEMENTARY NOTES

19. KEY WORDS *(Continue on reverse side if necessary and identify by block number)*

High frequency solutions
Electromagnetic radiation
Large aperture antennas
Large arrays
Radiation obstacles
Low scattering levels
Analytic solutions

20. ABSTRACT *(Continue on reverse side if necessary and identify by block number)*

The Geometrical Theory of Diffraction (GTD) has been used for more than a decade to compute the radiation patterns of antennas. A significant portion of that effort has been directed toward computing patterns for antennas mounted in complex environments such as aircraft or ships. As a result of various successes in treating such problems, it has been suggested here that GTD can be applied to similar problems in which the single antenna considered previously is replaced by a large array. In this

DD FORM 1 JAN 73 1473 EDITION OF 1 NOV 65 IS OBSOLETE

402251

SECURITY CLASSIFICATION OF THIS PAGE *(When Data Entered)*

20.

regard, this report demonstrates that GTD can successfully predict the low scattering associated with a pattern side lobe hitting a plate or set of plates. In that it is not pertinent what created the low side lobe which intersects the plate, a rectangular horn is used as the source in that it is much simpler to control experimentally. Based on many comparisons between calculated and measured results, it appears that GTD can accurately predict these low scattering levels, i.e., especially accurate for at least the first 20 dB below the maximum plate illumination level.

TABLE OF CONTENTS

		Page
I.	BACKGROUND	1
II.	THEORY	2
	2-1. Wedge Diffraction	2
	2-2. Horn E-plane Pattern Solution	10
	2-3. A Line Source Radiating in the Presence of a Strip	13
III.	ANALYSIS OF HORN/OBSTACLE FIELD PATTERNS	17
	3-1. Introduction	17
	3-2. Horn in the Presence of a Single Plate	17
	3-3. Analysis of Plate-to-Plate Interactions	20
IV.	CONCLUSIONS	36
REFERENCES		37

I. BACKGROUND

Since the Geometrical Theory of Diffraction (GTD) was introduced, the analysis of antenna radiation patterns has become more practical. This method gives one accurate information about the radiated fields even when obstacles are located near the antenna.

This report describes the GTD analysis of field patterns radiated by a horn antenna in the presence of perfectly conducting flat plates (i.e., obstacles). The basic approach applied in this study is to compute the radiation patterns for two different situations. The first one applies to only one plate, and the next one uses two plates.

In the case of one plate, the most significant terms are the incident field directly from the source, a reflected field from the plate and a singly diffracted field from each of the plate edges. But when two plates are used, additional terms such as a double reflected field, a reflected/diffracted field and a diffracted/reflected field are superimposed with the previously mentioned terms. These additional fields are caused by interactions between the plates.

The horn antenna patterns in this study are taken in the E-plane so that a two dimensional solution can be applied. Plates are mainly located outside the flare angle of the horn in order to observe how the plates affect the sidelobes or lower radiation levels. In other words, the whole radiation pattern in the presence of obstacles strongly depends on the complete geometry.

Various experimental results are used to verify the accuracy of the calculated patterns.

II. THEORY

2-1. Wedge Diffraction

A. Introduction

When a line source illuminates a wedge, the radiation from the source and scattering from the wedge can be analyzed by the GTD, a high frequency technique allowing a complicated structure to be approximated by basic canonical shapes. The GTD is a ray optical technique and, therefore, allows one to gain some physical insight into the various reflection and diffraction mechanisms involved. Consequently, one is able to quickly determine the most significant scattering mechanism for a given geometrical configuration. This, in turn, leads to an accurate engineering solution to practical antenna problems. The basic GTD solutions needed are discussed in this chapter, and these solutions are applied to specific structural scattering problems in the following chapters. For the geometry shown in Figure 2-1, the total field is expressed by

$$\bar{E}^T = \bar{E}^i u^i + \bar{E}^r u^r + \bar{E}^d. \qquad (2\text{-}1)$$

The field (E^i) is the electric field directly radiated by the source, the field ($\bar{E}^r$) is the electric field reflected from the surface of the obstacle, and the field ($\bar{E}^d$) is the diffracted field from the edges of the structure. The unit step functions u^i and u^r are shown to emphasize the discontinuities in the incident and reflected fields at the shadow boundaries. They are defined as being unity in the "so-called" lit regions and zero elsewhere. The extent of these regions is determined by Geometrical Optics (GO). The surfaces used in this report are perfectly conducting plates and the surrounding medium is free space.

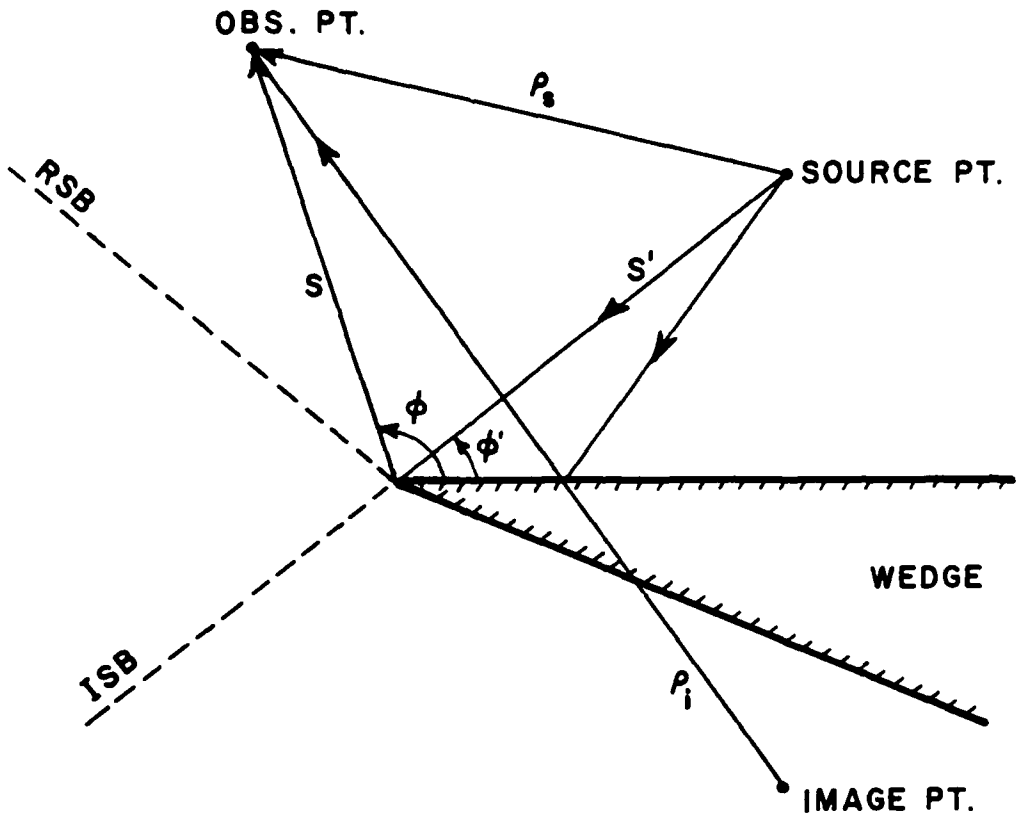

Figure 2-1. Basic wedge diffraction geometry.

B. Geometrical-Optics Fields

The incident field $\bar{E}^i$ (or $\bar{H}^i$) can be produced by a source causing a plane, cylindrical or spherical wave. Since a line source is used in this report, the incident field is defined by

$$\bar{E}^i = \begin{cases} \hat{z}\, C_1\, I\, \dfrac{e^{-jk\rho_s}}{\sqrt{\rho_s}} & , \quad 0^o \le \phi \le 180^o + \phi' \\ 0 & , \quad \text{otherwise} \end{cases} \tag{2-2}$$

where

$\bar{E}^i$ is the electric line source field,

and

$$C_1 = \frac{-kz_o e^{-j\pi/4}}{\sqrt{8\pi k}} \quad , \quad \text{with I being the electric current}$$

or

$$\bar{H}^i = \begin{cases} \hat{z}\, C_2\, M\, \dfrac{e^{-jk\rho_s}}{\sqrt{\rho_s}} & , \quad 0^o \le \phi \le 180^o + \phi' \\ 0 & , \quad \text{otherwise} \end{cases} \tag{2-3}$$

where

$\bar{H}^i$ is the magnetic line source field, and

$$C_2 = \frac{-ky_o e^{-j\pi/4}}{\sqrt{8\pi k}} \quad , \quad \text{with M being the magnetic current.}$$

Note that the lit region associated with the incident field is given by $0^o \le \phi \le 180^o + \phi'$ assuming $0^o \le \phi' \le 180^o$.

The reflected field from a perfectly conducting plate as shown in Figure 2-1 is given in terms of GO by

$$\bar{E}^r = \begin{cases} -\hat{z}\, C_1\, I\, \dfrac{e^{-jk\rho_i}}{\sqrt{\rho_i}} & , \quad 0^o \le \phi \le 180^o - \phi' \\ 0 & , \quad \text{otherwise} \end{cases} \tag{2-4}$$

for an electric line source, and

$$\bar{H}^r = \begin{cases} z\, C_2\, M\, \dfrac{e^{-jk\rho_i}}{\sqrt{\rho_i}} & , \quad 0^o \le \phi \le 180^o - \phi' \\ 0 & , \quad \text{otherwise} \end{cases} \tag{2-5}$$

for a magnetic line source. Note that the lit region for the reflected field is given by region, $0^{o} \leq \phi \leq 180^{o} - \phi'$.

C. Edge Diffraction

The GTD provides diffracted field solutions for a wedge, corner, etc. This section briefly discusses the edge diffraction problem.

An asymptotic solution for diffraction from a conducting wedge was first solved by Sommerfeld[1]. Originally, the GTD[2] as applied to diffraction by a wedge was based on plane wave diffraction coefficients. However, as shown in Reference 3 the use of cylindrical wave diffraction coefficients has been found necessary in the treatment of antennas. Consequently, different formulations of wedge diffraction have superceded the plane wave diffraction coefficients originally proposed by Keller. Pauli[4] introduced the V_B function as a practical formulation to the solution for a finite angle conducting wedge. Hutchins and Kouyoumjian[5,6], however, have presented a formula for the diffracted field, which significantly improves the accuracy over that obtained from Pauli's form.

This improved diffraction solution[5,6] is significantly better in the transition regions (near the incident and reflected shadow boundaries). It can be written in the form:

$$V_B(L,\beta,n) = I_{-\pi}(L,\beta,n) + I_{+\pi}(L,\beta,n) \qquad (2\text{-}6)$$

where

$$I_{\pm\pi}(L,\beta,n) \doteq \frac{e^{-j(kL+\pi/4)}}{jn\sqrt{2\pi}} \sqrt{a}\cot\left(\frac{\pi \pm \beta}{2n}\right) \times e^{jkLa} \int_{\sqrt{kLa}}^{\infty} e^{-j\tau^2}\, d\tau + [\text{higher order terms}] \quad . \qquad (2\text{-}7)$$

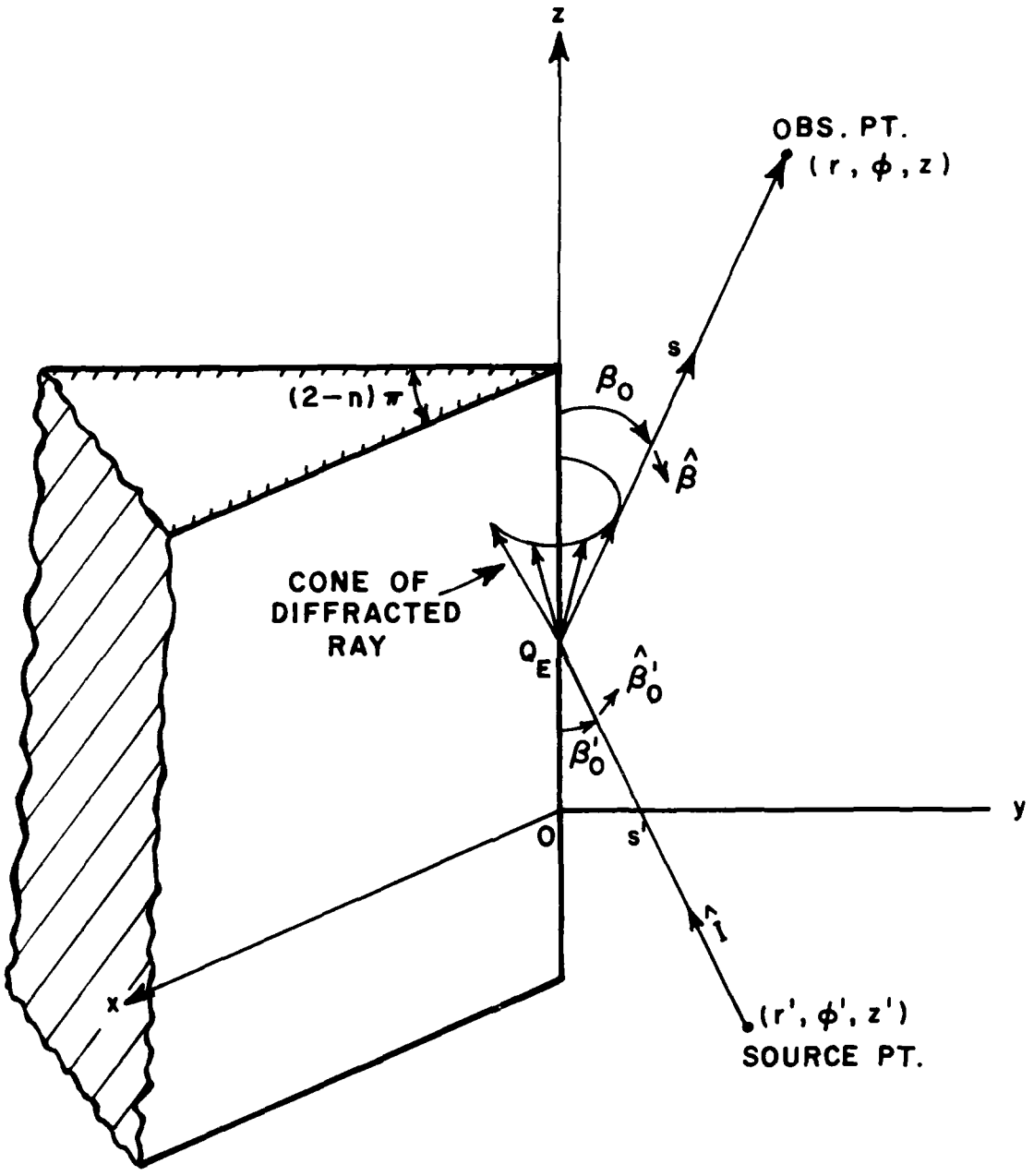

Figure 2-2. Geometry for three dimensional wedge diffraction problem.

Here the higher order terms are negligible for large kL. The parameter n is defined from the wedge angle relationship: WA = $(2-n)\pi$, $a^{\mp} = 1 + \cos(\beta - 2n\pi N^{\mp})$ where $N^{\mp}$ is a positive or negative integer or zero, whichever most nearly satisfies the equations

$$2n\pi N^{-} - \beta = -\pi \quad \text{for } I_{-\pi} \tag{2-8}$$

$$2n N^{+} - \beta = +\pi \quad \text{for } I_{+\pi} \ . \tag{2-9}$$

The variables L and β used here are defined below.

The wedge diffraction problem is illustrated in Figure 2-2. A source whose radiated $\bar{E}$ field is given by $\bar{E}^{i}$ is located at the point $s'(r',\phi',z')$. It can be an arbitrary electric or magnetic source causing plane, cylindrical, conical, or spherical wave incidence on the edge. The diffracted vector field at $s(r,\phi,z)$ can be written in terms of a dyadic diffraction coefficient. Kouyoumjian and Pathak[7] have given a more rigorous basis for the GTD formulation and have shown that the diffracted fields may be written compactly if they are in terms of an edge-fixed coordinate system centered at the point of diffraction (Q_E). The diffraction point is uniquely specified for a given source, edge and observation point. The incident ray diffracts as a cone of rays such that $\beta_0 = \beta_0'$.

The relationship between the orthogonal unit vectors associated with these coordinates (s', $\hat{\beta}_0'$, $\hat{\phi}'$; $\hat{s}$, $\hat{\beta}_0$, $\hat{\phi}$) are given by

$$\hat{I} = -\hat{s}' \tag{2-10}$$

$$\hat{I} = \hat{\beta}_0' \times \hat{\phi}' \tag{2-11}$$

$$\hat{s} = \hat{\beta}_0 \times \hat{\phi} \tag{2-12}$$

where $\hat{I}$ is the incident unit vector and $\hat{s}$ is the diffraction unit vector as shown in Figure 2-2.

The diffracted field is now given by

$$\bar{E}^d(s) \sim \bar{E}^i(Q_E) \cdot \bar{\bar{D}}_E(\hat{s},\hat{I})\, A(s)\, e^{-jks} \tag{2-13}$$

where

$$\bar{\bar{D}}_E = -\hat{\beta}_o'\,\hat{\beta}_o\,D_s - \hat{\phi}'\,\hat{\phi}\,D_h \tag{2-14}$$

$$D_{s,h}(\phi,\phi',\beta_o) = \frac{-e^{-j\pi/4}}{2n\sqrt{2\pi k}\,\sin\beta_o}\left[\cot\left(\frac{\pi+\beta^-}{2n}\right)F(kLa^+(\beta^-))\right.$$

$$+ \cot\left(\frac{\pi-\beta^-}{2n}\right)F(kLa^-(\beta^-)) \mp \left\{\cot\left(\frac{\pi+\beta^+}{2n}\right)\right.$$

$$\left.\left. F(kLa^+(\beta^+)) + \cot\left(\frac{\pi-\beta^+}{2n}\right)F(kLa^-(\beta^+))\right\}\right] , \tag{2-15}$$

and

$$F(x) = 2j|x|\, e^{jx} \int_{|\sqrt{x}|}^{\infty} e^{-j\tau^2}\, d\tau \quad . \tag{2-16}$$

Note that F(x) is called the transition function. In matrix notation this can oe written as

$$\begin{bmatrix} E_n^d(s) \\ E_\perp^d(s) \end{bmatrix} \sim \begin{bmatrix} -D_s & 0 \\ 0 & -D_h \end{bmatrix} \begin{bmatrix} E_n^i(Q_E) \\ E_\perp^i(Q_E) \end{bmatrix} A(s)\, e^{-jks} \tag{2-17}$$

The D_s coefficient applies for the case of the E-field component being parallel to the edge (electric line source) with the boundary condition (acoustically soft)

$$(\bar{E}|_{wedge}) = 0 \quad . \tag{2-18}$$

The D_h coefficient applies when the $\bar{E}$-field vector is perpendicular to the edge (magnetic line source) with the boundary condition (acoustically hard)

$$(\frac{\partial \bar{E}}{\partial \bar{n}}) = 0 \quad . \tag{2-19}$$

The angular relations are expressed by

$$\beta = \beta^{\pm} = \phi \pm \phi' \quad . \tag{2-20}$$

The $\phi-\phi'$ term is related to the incident field, and the $\phi+\phi'$ term is associated with the reflected field. The quantity A(s) is the ray divergent factor given by[8]

$$A(s) = \begin{cases} \frac{1}{\sqrt{s}} & \text{plane, cylindrical wave incidence} \\ \sqrt{\frac{s'}{s(s'+s)}} & \text{spherical wave incidence} \end{cases} \tag{2-21}$$

Here the distance parameter (L) for a straight wedge is given by[8]

$$L = \begin{cases} s \sin^2\beta_o & \text{plane wave incidence} \\ \frac{ss'}{s+s'} & \text{cylindrical wave incidence} \\ \frac{ss'\sin^2\beta_o}{s+s'} & \text{conical and spherical wave incidence} \end{cases} \tag{2-22}$$

At grazing incidence (i.e., when $\phi'=0$), the expression for D_h and D_s must be multiplied by a factor of 1/2. This comes about because the incident and reflected fields merge together and only one-half the total field on the surface is associated with the incident field, the other half being the reflected field.

2-2. Horn E-plane Pattern Solution

The E-plane radiation pattern for a rectangular horn can be analyzed using GTD as suggested by Russo et al[3].

Since a rectangular horn antenna has two diffractions in addition to the radiation from the horn throat, one can analyze the E-plane pattern using the three radiation mechanisms illustrated in Figure 2-3.

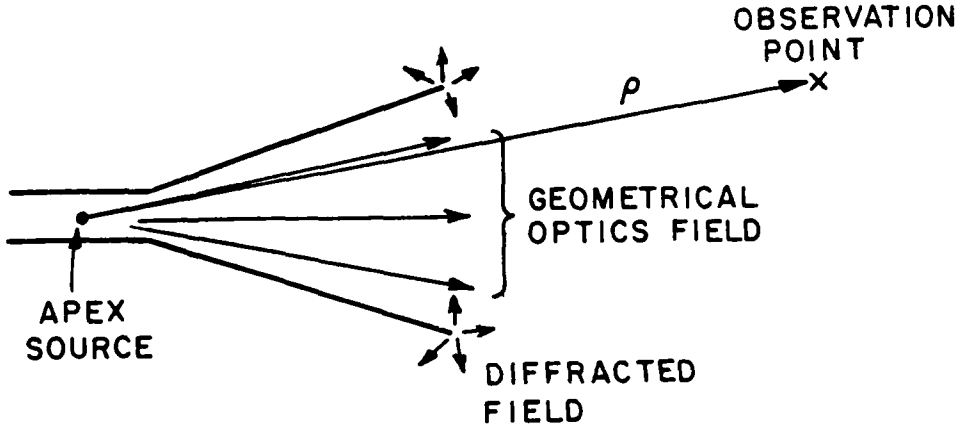

Figure 2-3. GTD horn radiation terms.

Fields from the apex source are obtained by the GO method. This field is confined to the horn flare angle and the amplitude and phase are only dependent upon the radial distance (ρ) as shown in Figure 2-3. The total GO field is represented by the one source at the horn apex.

Next, diffracted fields from the horn edges are considered. Since $\phi'=0$ and the grazing incidence case exists, the diffraction coefficients are

$$D_h(\phi,\beta_o) = - \frac{e^{-j\pi/4}}{2n\sqrt{2\pi k}\sin\beta_o} \left[\cot\left(\frac{\pi+\phi}{2n}\right) F(kLa(\beta)) + \cot\left(\frac{\pi-\phi}{2n}\right) F(kLa(\beta))\right] . \quad (2\text{-}23)$$

Therefore, the total far zone field of a horn antenna can be derived as follows.

From Figure 2-4,

$$\phi_1 = \pi/2 - \theta_o + \theta \quad (2\text{-}24)$$

$$\phi_2 = 3/2\,\pi - \theta_o - \theta \quad (2\text{-}25)$$

$$\rho_1 = \rho - \rho_o \sin(\theta - \theta_o) \quad (2\text{-}26)$$

$$\rho_2 = \rho - \rho_o \sin(\theta + \theta_o) \quad (2\text{-}27)$$

$$E_{TOT} = E^{GO} + E_1^d + E_2^d \quad (2\text{-}28)$$

$$= CK\left[\frac{e^{-jk\rho}}{\rho} + E^i(Q_{1,2})\left(D_{h_1}\frac{e^{-jk\rho_1}}{\sqrt{\rho_1}} + D_{h_2}\frac{e^{-jk\rho_2}}{\rho_2}\right)\right] \quad (2\text{-}29)$$

where

$$E^{i}(Q_{1,2}) = \frac{e^{-jk\rho_o}}{\sqrt{\rho_o}} \quad . \tag{2-30}$$

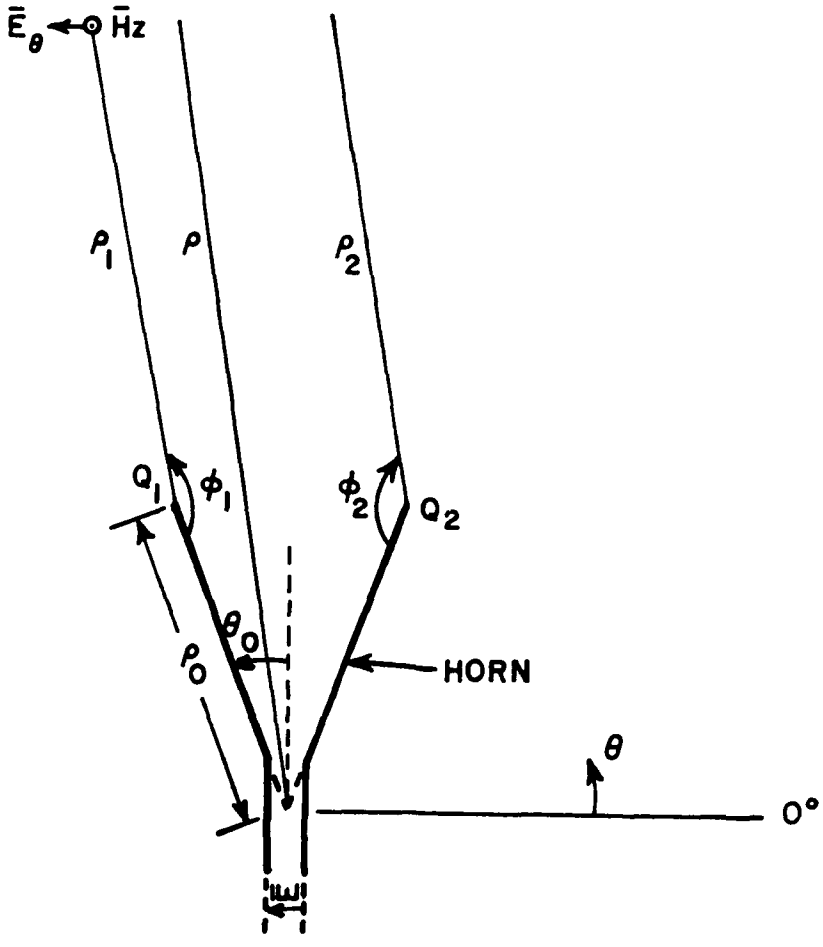

Figure 2-4. Geometry associated with horn analysis.

Hence, the total field of a magnetic line source in the far zone from Equation (2-29) is given by

$$E_{TOT} = CK \frac{e^{-jk\rho}}{\sqrt{\rho}} \left[u^i + \frac{e^{-jk\rho_o}}{\sqrt{\rho_o}} \left(D_{h_1} e^{jk\rho_o(\sin(\theta-\theta_o)} u_1^d \right.\right.$$

$$\left.\left. + D_{h_2} e^{jk\rho_o(\sin(\theta+\theta_o)} \right) u_2^d \right] . \qquad (2\text{-}31)$$

Figure 2-5 shows an ideal (computed) radiation pattern with both sides symmetric about the axis at 90^o.* The measured curve here almost coincides with the computed curve. The main lobe shows excellent agreement, and the first sidelobes are with a decibel. However the measured pattern behind the horn is not as smooth as the computed curve and there is a 4 dB difference at 270^o. This results in that the computed curve does not include diffractions from an input connector and the pyramidal structure at the back of the horn.

2-3. A Line Source Radiating in the Presence of a Strip

Before proceeding to the more difficult problem of analyzing antennas in the presence of complex structures, let us consider the GTD analysis of a single line source radiating in the presence of a perfectly conducting strip as shown in Figure 2-6. Geometrical-optics fields and diffracted fields from the conducting strip are treated by the GTD.

In order to simplify the problem, the line source is assumed parallel with the strip edges, allowing a two dimensional coordinate system to be used. The case of the conducting strip is equivalent to

*Analyzing Figure 2-5, it is noted that the main lobe is caused primarily by geometrical optics fields generated by the apex source within the limited horn flare angles. The first sidelobes are caused by the diffraction effects of the horn edges.

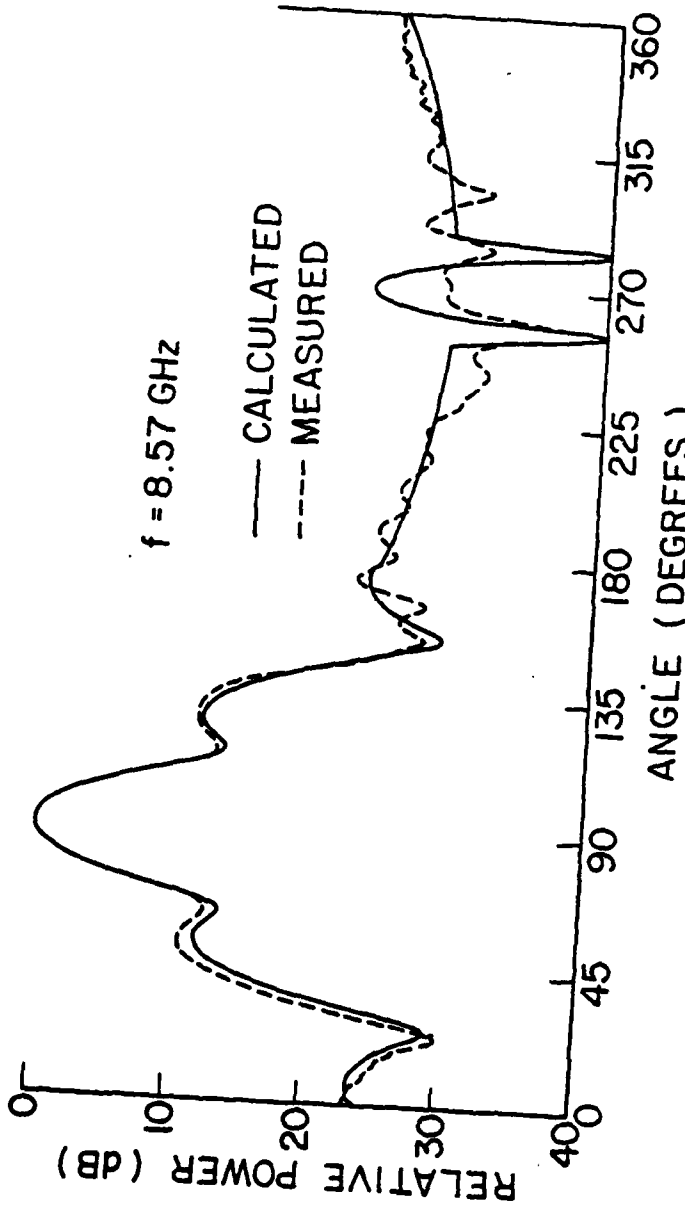

Figure 2-5. Comparison of computed and measured horn E-plane patterns.

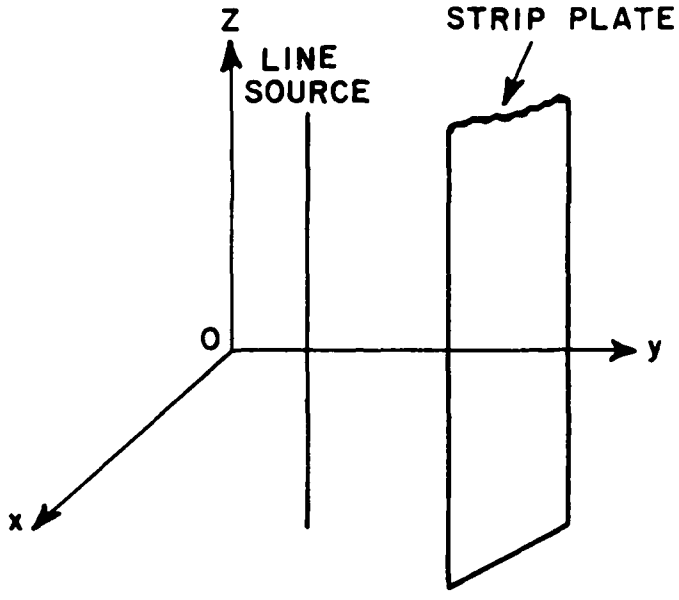

(a) 3 DIMENSIONS

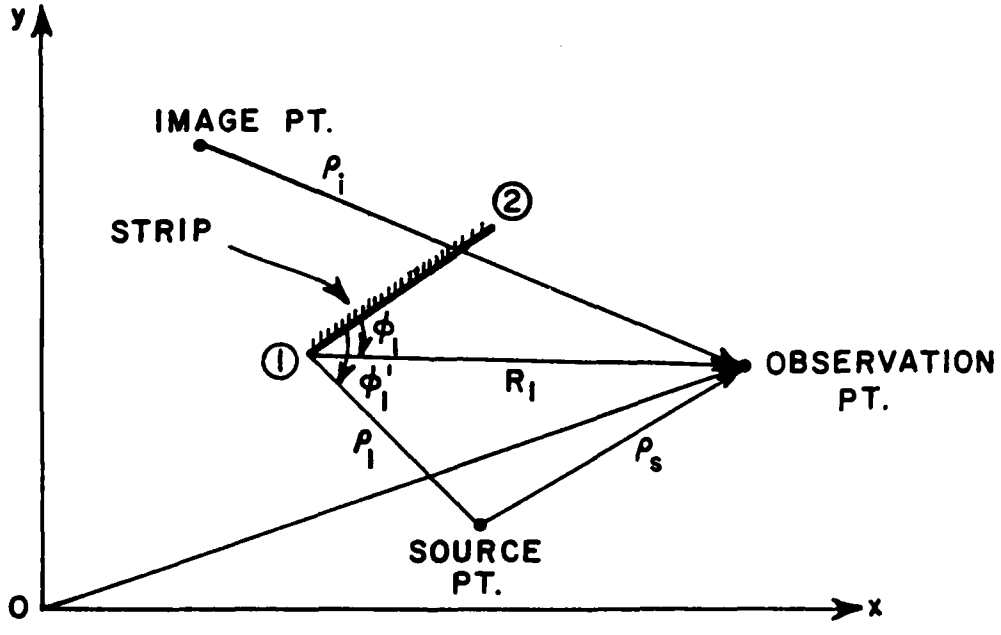

(b) 2 DIMENSIONS

Figure 2-6. Geometry associated with strip diffraction problem.

two half planes or two edges with both wedge angles zero. Thus the total field for a line source near a strip is given by

$$\bar{E}^T = \bar{E}^i u^i + \bar{E}^r u^r + \bar{E}_1^d + \bar{E}_2^d \tag{2-32}$$

Here $\bar{E}_1^d$ is the diffracted field from edge 1 , and $\bar{E}_2^d$ is the diffracted field from edge 2 . The unit step functions u^i and u^r are unity in lit regions and zero otherwise. Referring to Figure 2-6, the various field terms can be expressed by

$$\bar{E}^i u^i = \hat{z}\, C\, \frac{e^{-jk\rho_s}}{\sqrt{\rho_s}}\, u^i \tag{2-33}$$

$$\bar{E}^r u^r = \pm\, \hat{z}\, C\, \frac{e^{-jk\rho_i}}{\sqrt{\rho_i}}\, u^r \tag{2-34}$$

$$\bar{E}_1^d = \hat{z}\, C\, \{D_{h_s}(\phi_1-\phi_1') \pm D_{h_s}(\phi_1+\phi_1')\}\, \frac{e^{-jk\rho_1}}{\sqrt{\rho_1}}\, \frac{e^{-jkR_1}}{\sqrt{R_1}} \tag{2-35}$$

$$\bar{E}_2^d = \hat{z}\, C\, \{D_{h_s}(\phi_2-\phi_2') \pm D_{h_s}(\phi_2+\phi_2')\}\, \frac{e^{-jk\rho_2}}{\sqrt{\rho_2}}\, \frac{e^{-jkR_2}}{\sqrt{R_2}} \tag{2-36}$$

III. ANALYSIS OF HORN/OBSTACLE FIELD PATTERNS

3-1. Introduction

This chapter describes the analysis of the radiation patterns of horn antennas in the presence of conducting plates (i.e., obstacles) using the GTD.

The horn radiation is treated using the analysis presented in Section 2-3 in which the horn antenna is simulated by an array of 3 magnetic line sources (i.e., apex plus 2 edge diffractions as shown in Section 2-2).

The horn antenna patterns are taken in the E-plane with all the plates aligned perpendicular to that pattern cut such that one can apply a two dimensional analysis to this three dimensional problem. In order to illustrate all the pertinent GTD terms the radiated fields are computed and measured for two different situations (one and two plate obstacles).

3-2. Horn in the Presence of a Single Plate

Based on the GTD, one can extend the horn analysis of the previous chapter to treat the problem of a strip in the presence of a horn. Note that the three horn sources (throat radiation, plus two edge diffractions) may illuminate the strip. In that low level radiation prediction is being studied here. It is assumed that the plate cannot be illuminated by the throat radiation. Thus only diffracted fields from the horn edges hit the plate as shown in Figure 3-1.

Analyzing the field pattern for the horn and plate in detail, the total field ($\bar{E}^t$) is expressed by

$$\bar{E}^t = \bar{E}^s + \bar{E}^r + \bar{E}^d \qquad (3\text{-}1)$$

where

$\bar{E}^s$ = Source field from the horn
$\bar{E}^r$ = Reflected field from the plate
$\bar{E}^d$ = Diffracted field from plate edges

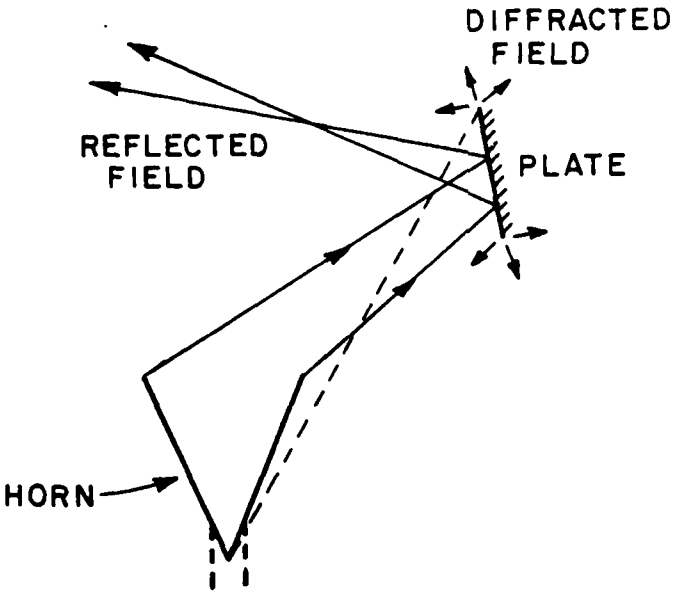

Figure 3-1. Horn in the presence of a single plate.

As discussed above, the field $\bar{E}^s$ is composed of geometrical optics fields from the horn apex and diffracted fields from the horn edges. These two different fields have their own shadow and lit regions according to the horn geometry.

Since the plate in this report is located outside the horn flare angle, the geometrical optics field does not hit the plate; whereas, the diffracted fields from the horn edges do. Thus, the reflected fields shown in Figure 3-2 can be expressed as

$$\bar{E}^r = \bar{E}_1^r u_1^r + \bar{E}_2^r u_2^r$$

$$= \sum_{m=1}^{2} u_m^r D_h(\phi_m) \exp[-jk(\rho_{im}+\rho_o)] / \sqrt{\rho_{im}} / \sqrt{\rho_o} \quad ; \qquad (3\text{-}2)$$

$$u_m^r = \begin{cases} 1 & \text{reflection region for the } \underline{m}\text{th diffraction, and} \\ 0 & \text{otherwise.} \end{cases}$$

Note that the constants and unit vectors discussed in Chapter 2 are omitted here.

Figure 3-2 shows the geometrical direction of the reflected fields when the diffracted fields from the horn edge ① hit the plate. The total reflected field, which includes the reflected field associated with diffractions from edges ① and ② of the horn, is shown in Figure 3-5(b) for the geometry illustrated in Figure 3-4. The diffracted fields from the plate edges (which are actually double diffracted fields) $\bar{E}^d$ can be expressed by Equation (3-3) and shown in Figure 3-3. These fields are given by

$$\bar{E}^d = \sum_{m=1}^{2} \sum_{\ell=1}^{2} D_h(\phi_{m\ell}) \; D_h(\alpha_\ell - \alpha_\ell') + D_h(\alpha_\ell + \alpha_\ell')$$

$$\exp[-jk(\rho_{m\ell}+R_\ell+\rho_o)] / \sqrt{\rho_m} / \sqrt{R_\ell} / \sqrt{\rho_o} \quad . \qquad (3\text{-}3)$$

Again an example of total diffracted is shown in Figure 3-5(c). The total field expressed by Equation (3-1) is shown in Figure 3-5(d). Computed and measured field patterns are shown in Figures 3-6, 3-7 and 3-8 for different frequencies.

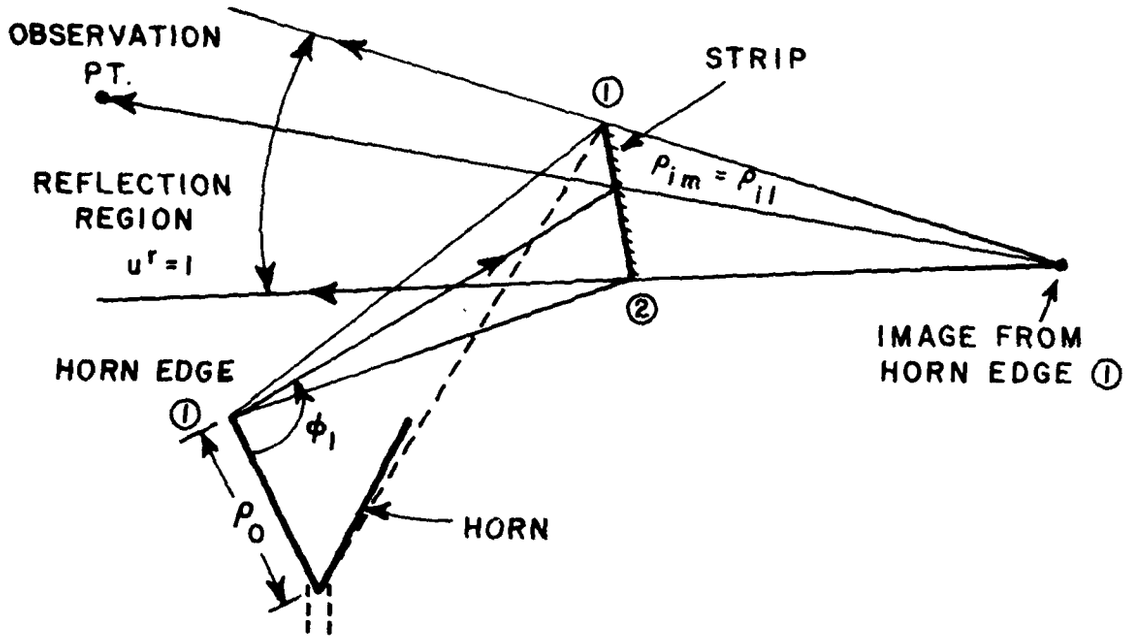

Figure 3-2. Reflection from plate near horn.

3-3. Analysis of Plate-to-Plate Interactions

In the case of two plates near a horn antenna, one must consider more complicated scattering mechanisms. That is higher order fields, which result from interactions between two plates, are added to the total field solution discussed in the previous section.

Considering the geometry shown in Figure 3-9, three significant terms (double reflected, reflected/diffracted and diffracted/reflected fields)[8] in addition to the source, reflected and diffracted fields must be computed. Thus, the total field ($\bar{E}^t$) for the two-plate case is given by

$$\bar{E}^t = \bar{E}^s + \bar{E}^r + \bar{E}^d + \bar{E}^{rr} + \bar{E}^{rd} + \bar{E}^{dr} \qquad (3\text{-}4)$$

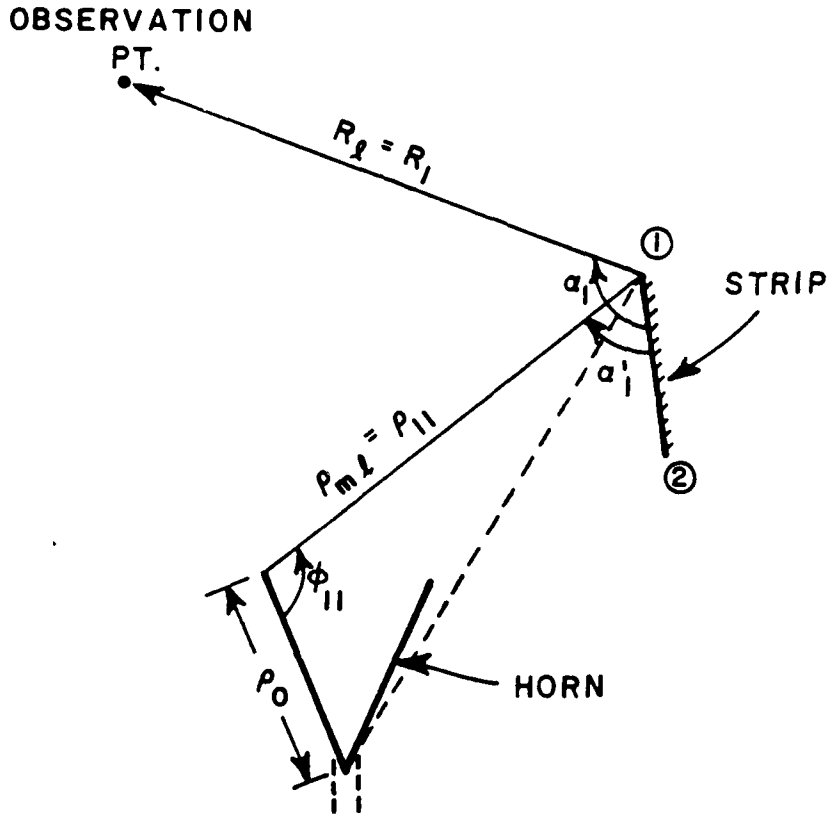

Figure 3-3. Diffraction from plate edge illuminated by a horn sidelobe in the E-plane.

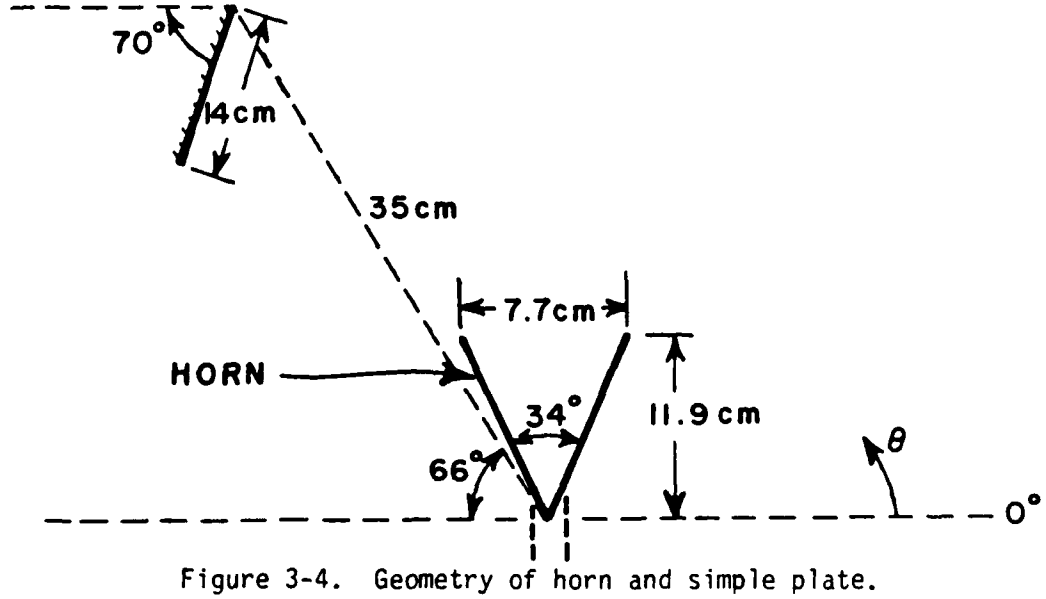

Figure 3-4. Geometry of horn and simple plate.

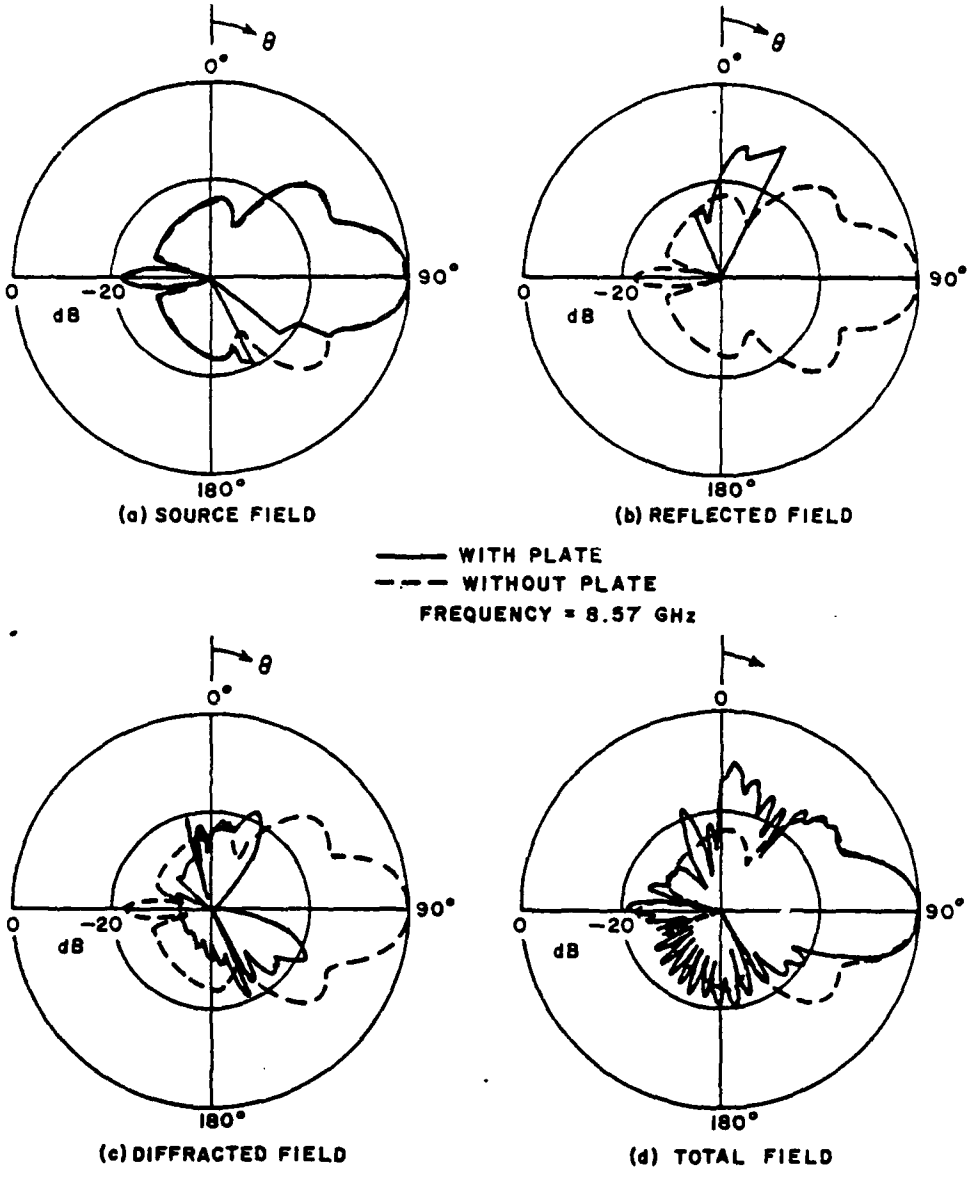

Figure 3-5. Calculated E-plane patterns of various GTD field terms associated with horn-to-plate interaction.

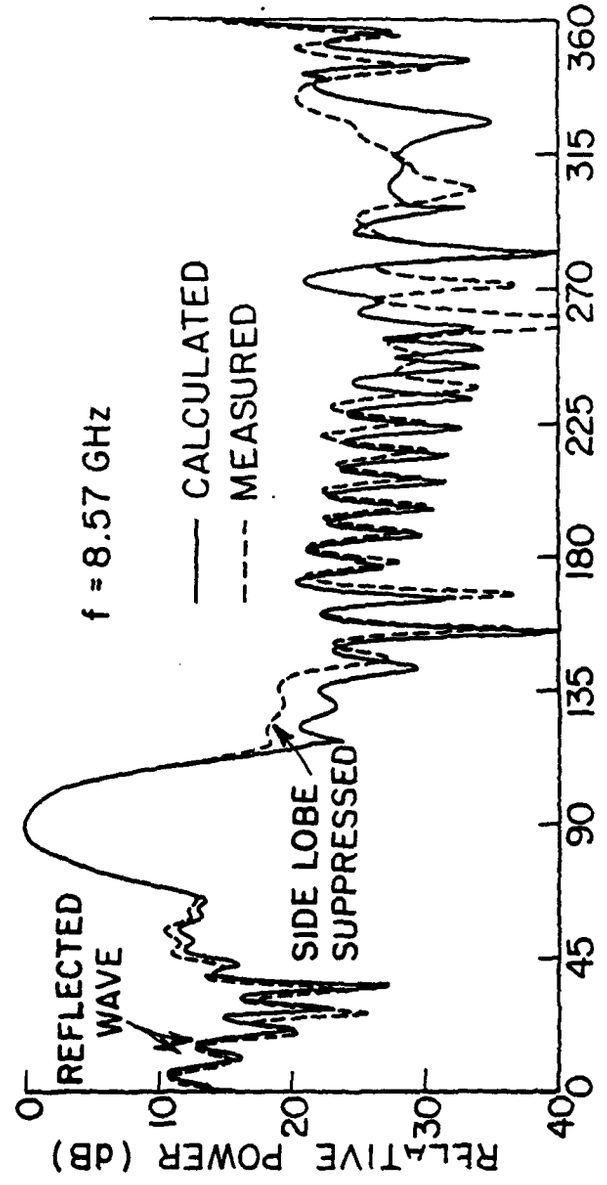

Figure 3-6. Comparison of computed and measured E-plane patterns for a horn in the presence of a single plate.

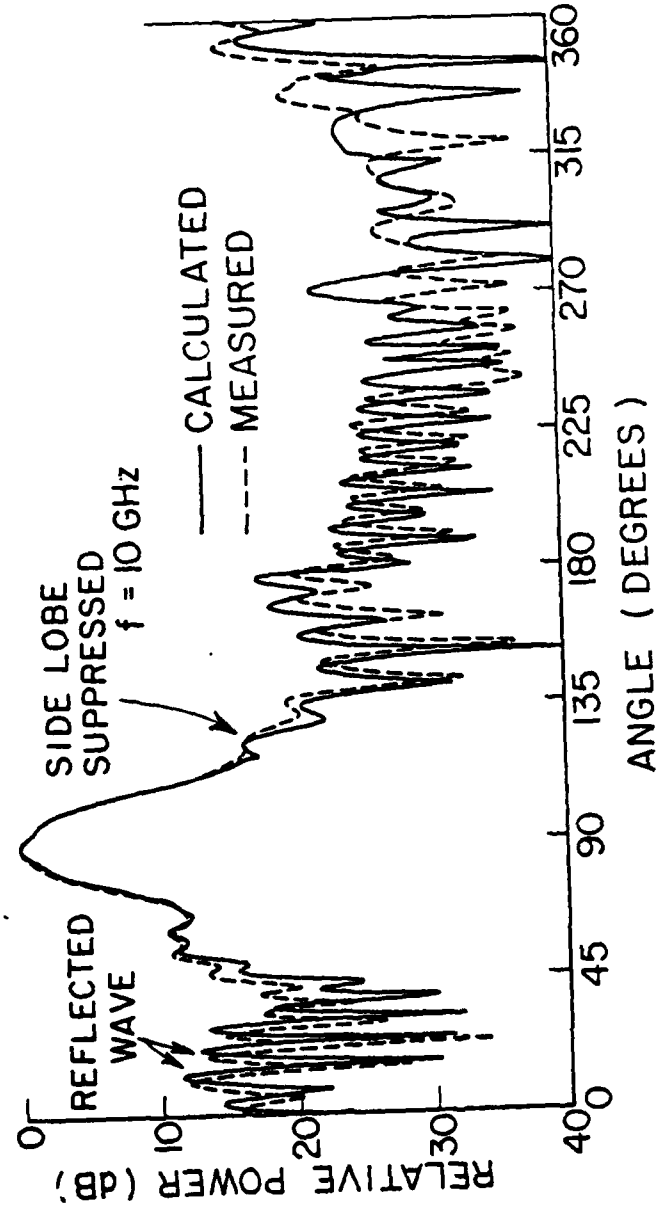

Figure 3-7. Comparison of computed and measured E-plane patterns for a horn in the presence of a single plate.

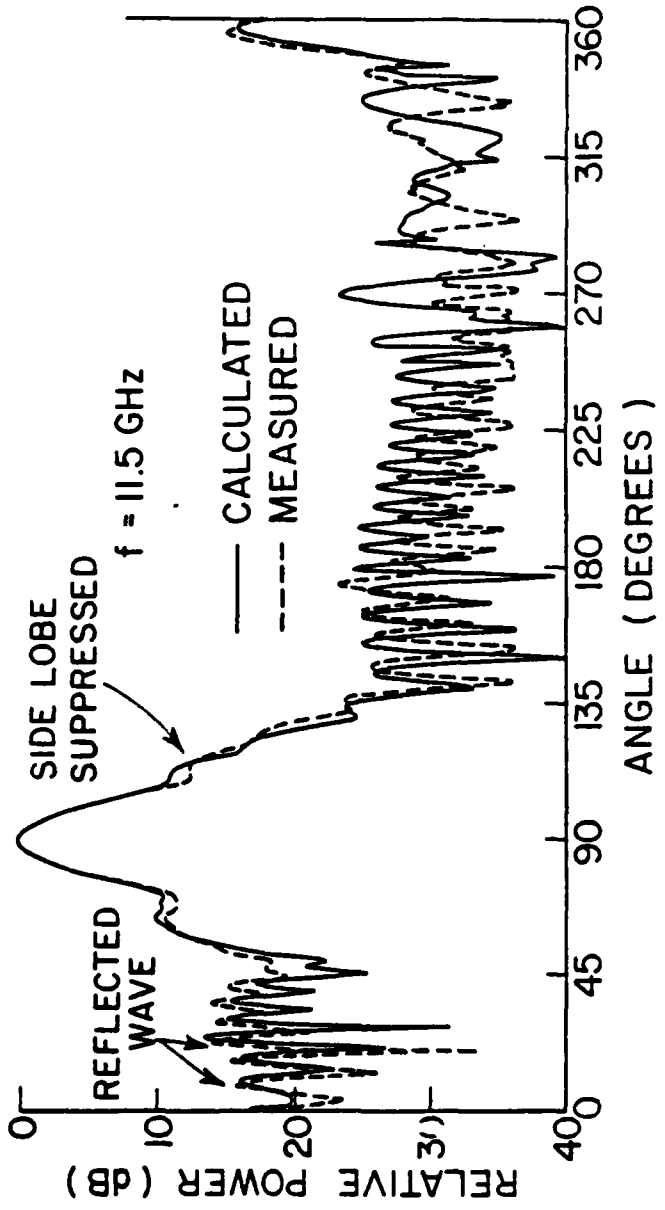

Figure 3-8. Comparison of computed and measured E-plane patterns for a horn in the presence of a single plate.

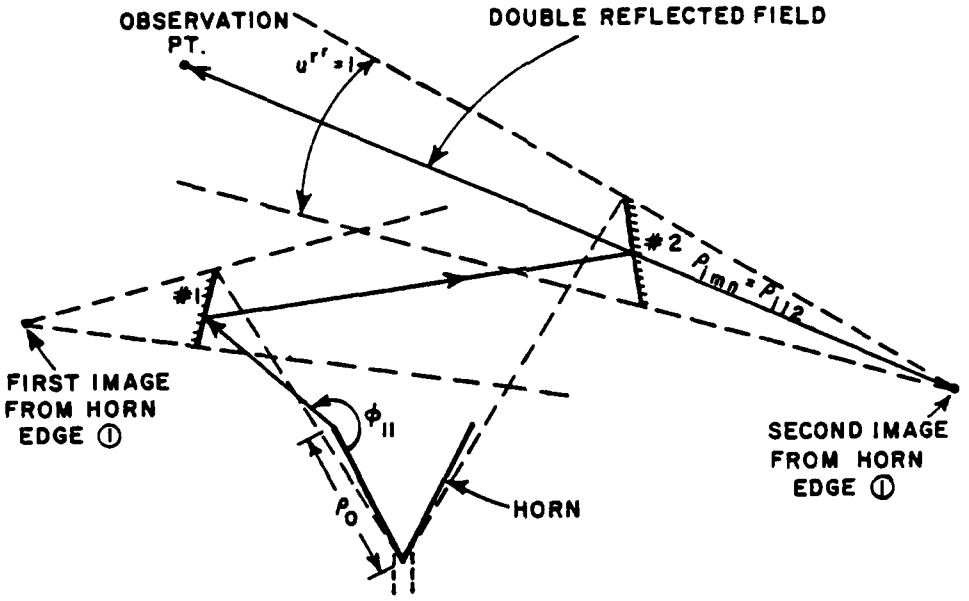

Figure 3-9(a). Double reflection from plate to plate.

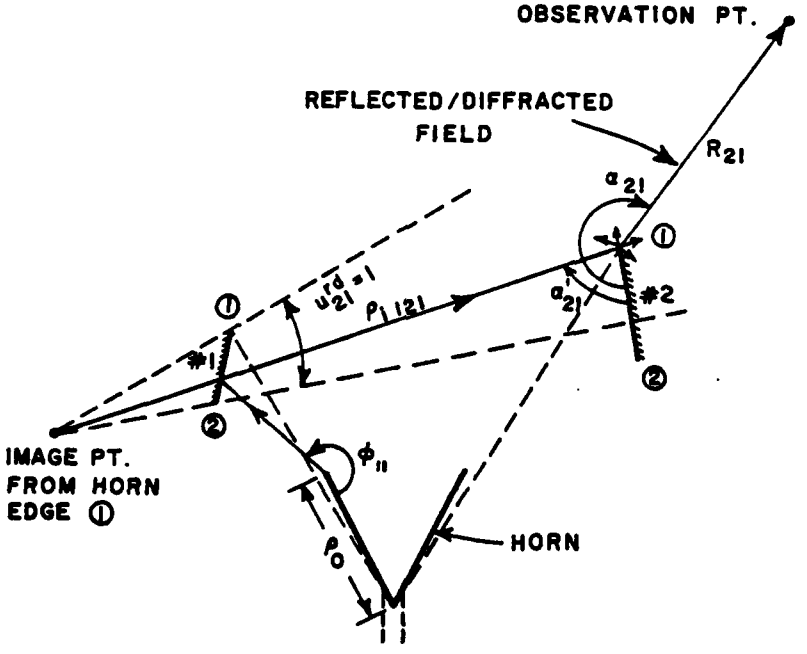

Figure 3-9(b). Reflected/diffracted field.

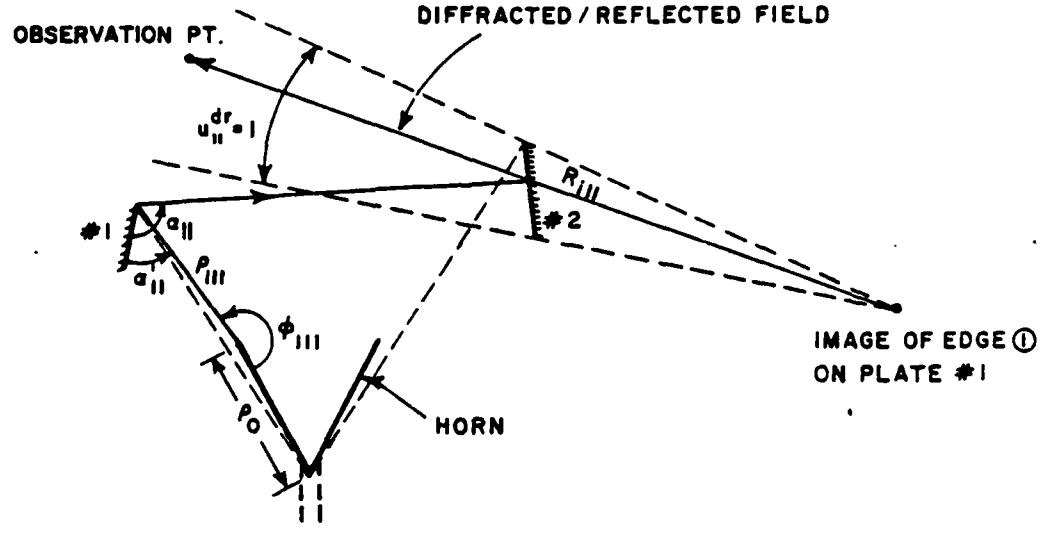

Figure 3-9(c). Diffracted/reflected field.

where $\bar{E}^{rr}$ = double reflected field off a plate after reflection by another plate,

$\bar{E}^{rd}$ = diffracted field off an edge after reflection by a plate (reflected/diffracted field), and

$\bar{E}^{dr}$ = reflected field off a plate after diffraction by a plate edge (diffracted/reflected field).

Figure 3-9 illustrates these various field mechanisms in terms of geometric illustrations. The doubly reflected field is given by

$$\bar{E}^{rr} = \sum_{m=1}^{2} \sum_{n=1}^{2} u_{mn}^{rr} D_h(\phi_{mn}) \exp(-jk(\rho_o+\rho_{imn}))/\sqrt{\rho_o}\sqrt{\rho_{imn}} \qquad (3\text{-}5)$$

u_{mn}^{rr} $\begin{cases} 1 & \text{double reflection region, and} \\ 0 & \text{otherwise.} \end{cases}$

Figure 3-9(a) illustrates a double reflection term in which a reflected field of horn edge ① reflects from plate #1 and, subsequently, is reflected from plate #2. Thus, some of the reflected energy from plate #1 intersects the other plate such that a new reflected wave, called a double reflected field, is created. Accordingly, the amplitude and phase of this wave is different as expressed by Equation (3-5). The reflected/diffracted field is given by

$$\bar{E}^{rd} = \sum_{m=1}^{2} \sum_{n=1}^{2} \sum_{\ell=1}^{2} u_n^{rd} D_h(\phi_{mn}) \left[D_h(\alpha_{n\ell} - \alpha'_{n\ell}) + D_h(\alpha_{n\ell} + \alpha'_{n\ell}) \right]$$

$$\exp\left[-jk(\rho_o + \rho_{imn} + R_{n\ell})\right] / \sqrt{\rho_o} / \sqrt{\rho_{imn\ell}} / \sqrt{R_{n\ell}} \quad . \qquad (3\text{-}6)$$

This field occurs when a reflected field from one plate hits an edge on the second plate. Figure 3-9(b) shows a reflected/diffracted wave produced when a reflected field via plate #1 hits edge ① on plate #2 in which case $u_{21}^{rd} = 1$.

Note that according to the geometry of Figure 3-9(b), $u_{22}^{rd} = 0$ in that edge ② on plate #2 is not illuminated by the reflected field from plate #1.

The total reflected/diffracted field is given by Equation (3-6), which is different than the diffracted field expressed by Equation (3-3) in that the field incident on the edge comes from a reflection mechanism.

Diffracted/reflected fields are the product of reflections from one plate after diffraction from another. This term is illustrated in Figure 3-9(c), and its solution is expressed by

$$\overline{E}^{dr} = \sum_{m=1}^{2} \sum_{n=1}^{2} \sum_{\ell=1}^{2} u_{n\ell}^{dr} D_h(\phi_{mn\ell}) \left[D_h(\alpha_{n\ell} - \alpha'_{n\ell}) \right.$$

$$\left. + D_h(\alpha_{n\ell} + \alpha'_{n\ell}) \right] \exp(-jk(\rho_o + \rho_{mn\ell} + R_{in\ell}))/\sqrt{\rho_o}/\sqrt{\rho_{mn\ell}}/\sqrt{R_{in\ell}} \quad (3\text{-}7)$$

On the basis of the above equations for each field component and using the geometry illustrated in Figure 3-10 the computed polar plots of each field component are illustrated in Figure 3-11(a)-(g) at a frequency of 11.5 GHz. Computed and measured results at different frequencies with the same geometry are, also, shown in Figures 3-12, 3-13 and 3-14.

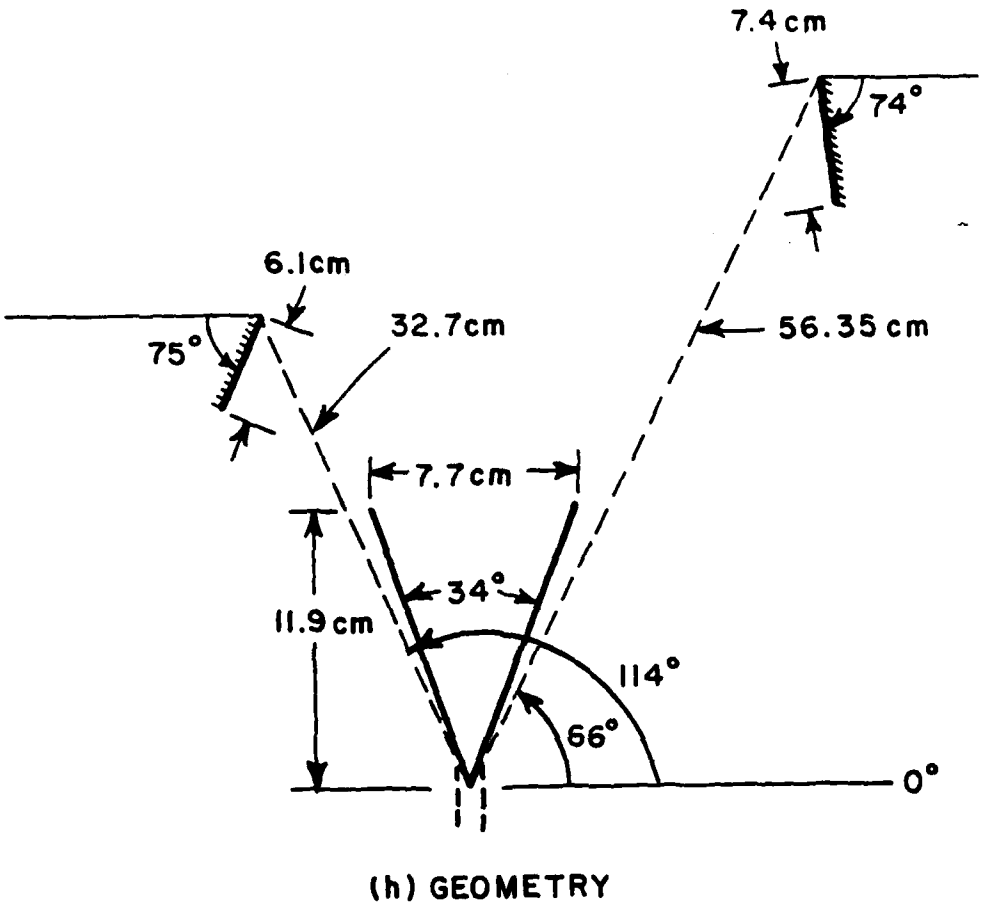

(h) GEOMETRY

Figure 3-10. Geometry of horn in presence of two plates.

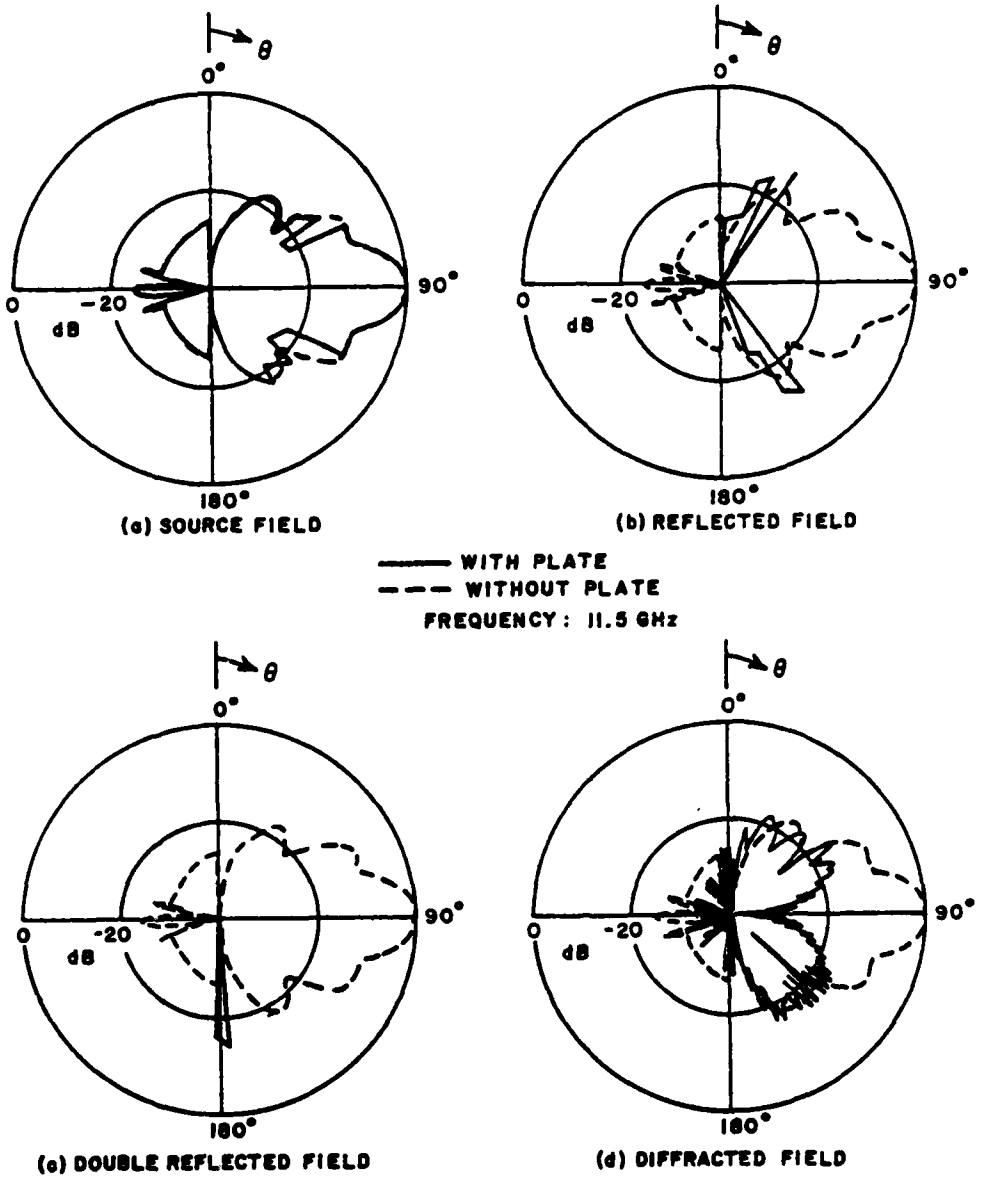

Figure 3-11. Calculated E-plane patterns of various GTD field terms associated with horn radiating in presence of two plates.

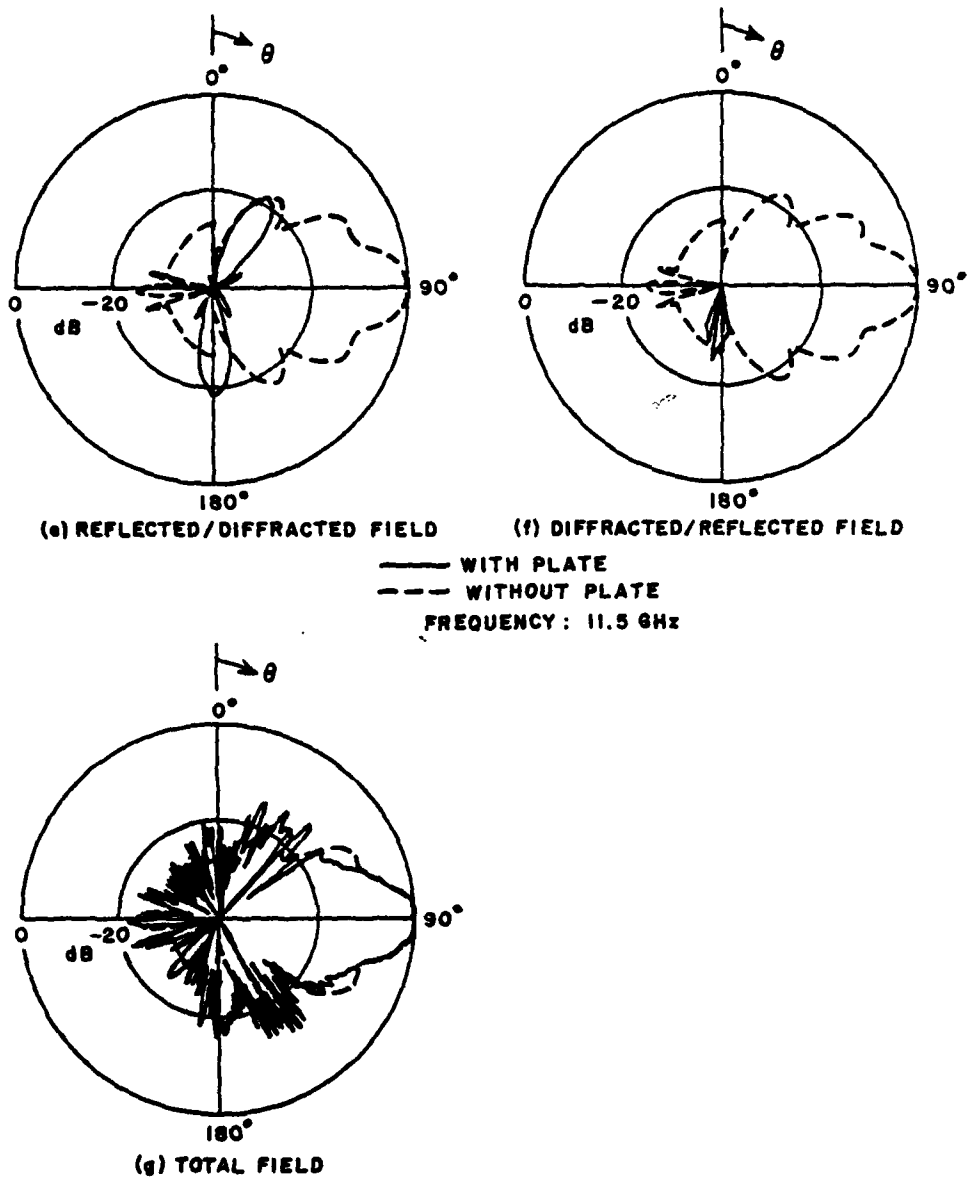

Figure 3-11 (continued).

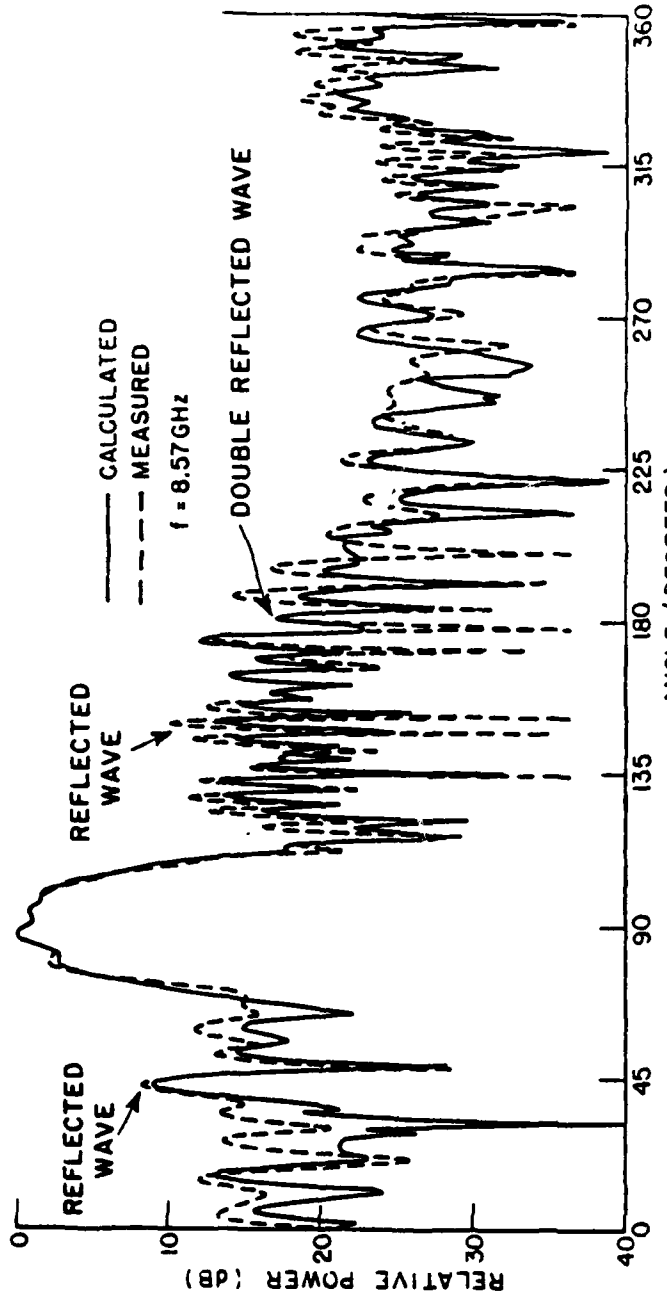

Figure 3-12. Comparison of computed and measured E-plane patterns for a horn in the presence of two plates.

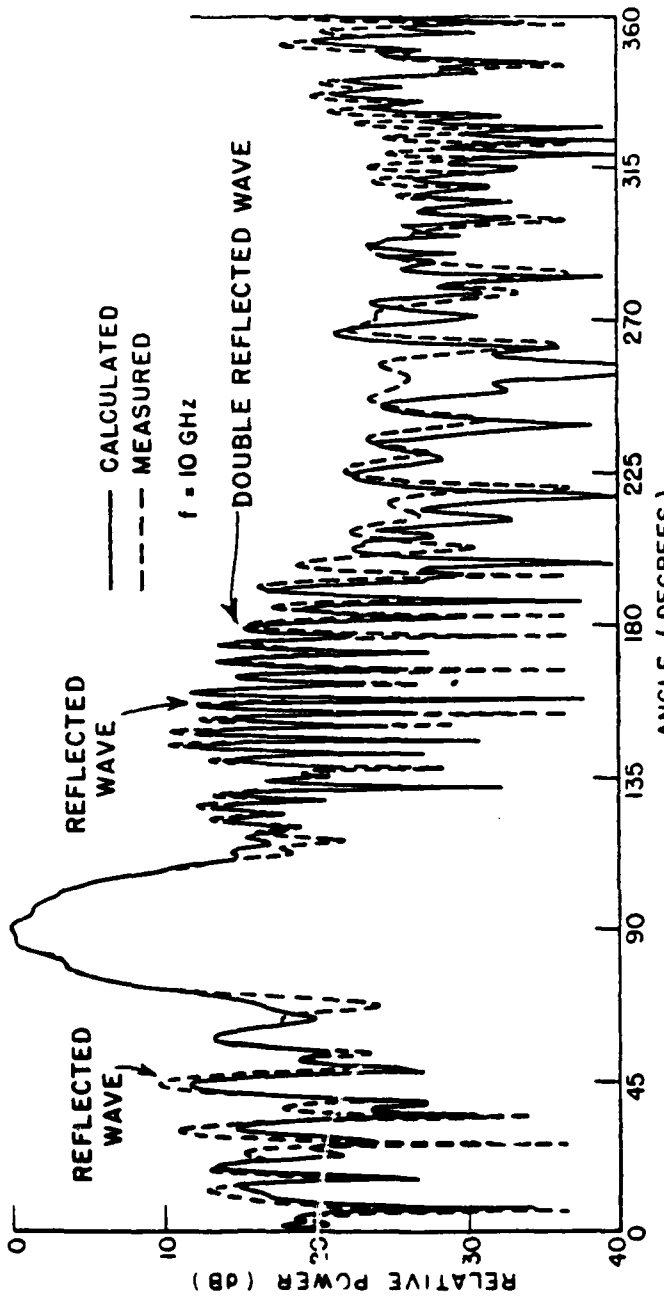

Figure 3-13. Comparison of computed and measured E-plane patterns for a horn in the presence of two plates.

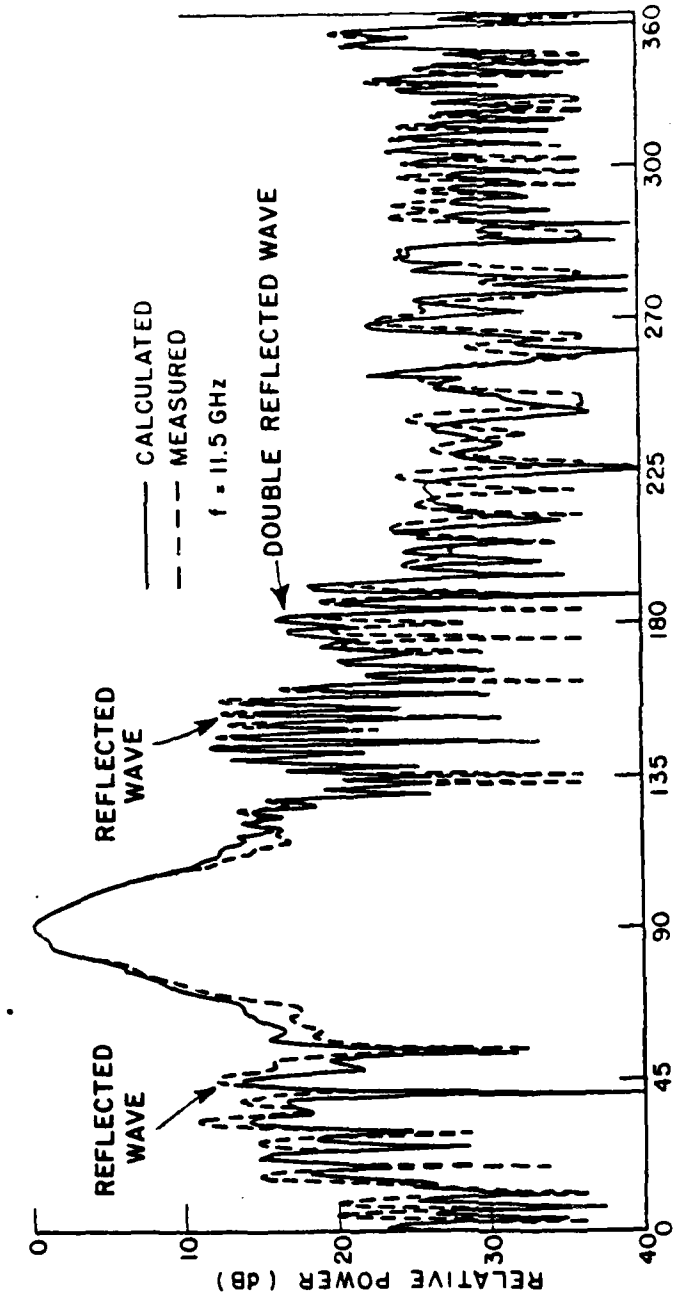

Figure 3-14. Comparison of computed and measured E-plane patterns for a horn in the presence of two plates.

IV. CONCLUSIONS

The purpose of this research effort has been to examine the utility of the Geometrical Theory of Diffraction (GTD) in analyzing the low scattering levels associated with large arrays mounted on aircraft. Specifically, can GTD accurately predict the scattering from an obstacle which is illuminated by a low side lobe associated with the radiation from a large array? To answer this question, the GTD has been used to analyze the scattering from a plate or set of plates illuminated by a side lobe from a rectangular horn. The horn is used here in that it is far simpler to use experimentally; yet, one can still illuminate structures with a side lobe. Using this approach various geometries were tested and compared with the GTD calculated results. It is our conclusion based on these comparisons that GTD can accurately predict the scattering from plates or plate simulated obstacles when they are illuminated by a side lobe radiated from a large aperture antenna or array.

REFERENCES

1. Sommerfeld, A., Optics, Academic Press, Inc., New York, 1954, pp. 245-265.

2. Keller, J. B., "Geometrical Theory of Diffraction", Jour. Optical Soc. Amer., 52 (February 1962), pp. 116-130.

3. Rudduck, R. C., "Application of Wedge Diffraction to Antenna Theory", Report 1691-13, 30 June 1965, The Ohio State University ElectroScience Laboratory, Department of Electrical Engineering; prepared under Grant NSF-338 for National Aeronautics and Space Administration, Washington, D.C. Also published as NASA Report CR-372.

4. Pauli, W., "An Asymptotic Series for Functions in the Theory of Diffraction of Light", Phys. Rev., 54 (1 December 1938), pp. 924-931.

5. Hutchins, D. L., "Asymptotic Series Describing the Diffraction of a Plane Wave by a Two Dimensional Wedge of Arbitrary Angle", Ph.D. Dissertation, The Ohio State University, Department of Electrical Engineering, 1967.

6. Hutchins, D. L., and Kouyoumjian, R. G., "A New Asymptotic Solution to the Diffraction by a Wedge", URSI 1967 Spring Meeting, Ottawa, Canada, pp. 154-155.

7. Pathak, P. H., and Kouyoumjian, R. G., "The Dyadic Diffraction Coefficient for a Perfectly Conducting Wedge", scientific report No. 5. Report 2183-4, 5 June 1970, The Ohio State University ElectroScience Laboratory, Department of Electrical Engineering; prepared under Contract AF19(628)-5929 for Air Force Cambridge Research Laboratories. (AFCRL-69-0546) (AD 707781).

8. Marhefka, R. J., "Analysis of Aircraft Wing-Mounted Antenna Patterns", Report 2902-25, June 1976, The Ohio State University ElectroScience Laboratory, Department of Electrical Engineering; prepared under Grant NGL 36-008-138 for National Aeronautics and Space Administration, Langley research Center, Hampton, Virginia.

DISTRIBUTION LIST

Report No. NADC-80095-30

	No. of Copies
DTIC	12
NADC, Code 8131	3
NADC, Code 3021	5